A study of a nonlinear filtering problem for tracking an extended target

Branko Ristic
DSTO
PO Box 1500
Edinburgh SA 5111
Australia
branko.ristic@dsto.defence.gov.au

David J. Salmond
QinetiQ
Cody Technology Park
Farnborough, Hants GU14 0LX
United Kingdom
djsalmond@qinetiq.com

Abstract − *The paper presents an analysis of a nonlinear filtering problem corresponding to tracking of an extended target whose shape is modelled by an ellipse. The measurements of target extent are assumed to be available in addition to the usual positional measurements. Using Cramer-Rao bounds we establish the best achievable error performance for this highly nonlinear problem. The theoretical bounds are used to examine the performance as a function of measurement accuracy, observer-target geometry and prior knowledge of shape parameters. Finally an extended Kalman filter (KF) and an unscented KF are developed for this application and their performance (consistency and RMS error) are examined.*

Keywords: Extended target, nonlinear filtering, Cramer-Rao bound, target tracking.

1 Introduction

A standard approach to target tracking is to assume a single point positional measurement corresponding to a target at each time step. Modern surveillance sensors, however, are able to supply (in addition to positional measurements), the measurements of target extent in one or two dimensions. For example a high resolution radar provides a useful measure of down-range extent given a reasonable target signal-to-noise ratio. Similarly, an imaging infra-red sensor can provide (at short ranges) an indication of angular target extent (or the cross-range extent).

The conventional tracking filters use the target centroid as a single point positional measurement and ignore this potentially useful additional information about the target extent [1]. More recent approaches to tracking extended targets use measurements of individual features or points on the target, by modelling object dynamics as a coordinated bulk motion [3], [10], [8] (for an overview see[9, Ch.11]). This approach, however, requires to deal with a complex issue of measurement to feature association.

In this study we take a different approach, recently proposed in [11]. The main idea is to adopt an elliptical model of target shape, which is suitable for example in maritime surveillance (tracking ships etc.). The elliptical model is convenient because both the target down-range and cross-range vary smoothly with orientation relative to the line-of-sight (LOS) between the observer and the target. The incorporation of the target (elliptical) shape parameters into the state vector, however, poses some difficulties for the resulting nonlinear filtering problem, as reported in [11]. In this study we examine in more depth this nonlinear filtering problem using the Cramér-Rao lower bound (CRLB) [9, Ch.4] as an analysis tool. Then an Extended Kalman filter (EKF) and an Unscented Kalman filter (UKF) are developed for this application. The error performance of these two nonlinear filters is compared to the theoretical CRLB and their consistency is analysed by normalised estimation error squared (NEES) [2].

It is important to emphasise that the purpose of using target extent measurements in a tracking system is not so much to improve the track accuracy, but more importantly to estimate a very useful target feature: the major and minor axes of its (elliptical) shape. These target shape estimates are extremely useful both for track maintenance [11] (e.g. in dense target/false alarm environments) and for target identification.

The remaining part of the paper is organised as follows. Section 2 presents a mathematical formulation of the nonlinear filtering problem for tracking an ellipsoidal target using measurements of its position and extent. Section 3 describes the derivation of the theoretical CRLB for this nonlinear filtering problem. Section 4 is devoted to an analysis of CRLB as a function of measurement accuracy, target-observer geometry and the influence of prior knowledge of shape parameters. Section 5 presents an analysis of EKF and UKF error performance. Section 6 summarises the main results of this study.

2 Problem statement

Let us consider an extended target moving in the x-y plane, whose shape can be modelled by an ellipse. A typical scenario of interest is shown in Figure 1. The observer and target kinematic state vectors are defined as:

$$\mathbf{x}^o = \begin{bmatrix} x^o & \dot{x}^o & y^o & \dot{y}^o \end{bmatrix}^T \quad (1)$$

$$\mathbf{x}^t = \begin{bmatrix} x^t & \dot{x}^t & y^t & \dot{y}^t \end{bmatrix}^T \quad (2)$$

respectively. Here (x, y) is the position and $(\dot{x}, \dot{y})$ is the velocity in the Cartesian x-y plane. The observer kinematic state is assumed to be known. The relative kinematic state vector is then:

$$\mathbf{x} = \mathbf{x}^t - \mathbf{x}^o = \begin{bmatrix} x & \dot{x} & y & \dot{y} \end{bmatrix}^T. \quad (3)$$

Our goal is to estimate the *joint* kinematic-feature state vector:

$$\mathbf{y} = \begin{bmatrix} \mathbf{x}^T & \ell & \gamma \end{bmatrix}^T \quad (4)$$

where ℓ is the target length (i.e. the length of the major axis of its corresponding ellipse) and $\gamma < 1$ is the quotient of target width and length (i.e. the ratio of minor and major axes of the ellipse). The down-range and cross-range extent of an ellipsoidal target can then be expressed as (see Figure 1):

$$L(\phi) = \ell\sqrt{\cos^2\phi + \gamma^2 \sin^2\phi} \quad (5)$$

$$W(\phi) = \ell\sqrt{\sin^2\phi + \gamma^2 \cos^2\phi}, \quad (6)$$

where ϕ is the angle between the major axis of the ellipse and the target-observer LOS.

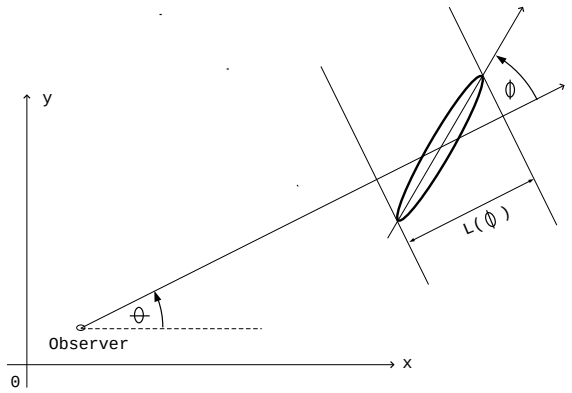

Fig. 1: Observer – Extended Target geometry in x-y plane

2.1 State dynamics

In order to simplify analysis, we consider the case where the target is moving with a nearly constant velocity motion [2]. In general, however, this is not necessary (e.g. [11] considers coordinated turn model). The discrete-time state dynamic equation can be written as:

$$\mathbf{y}_{k+1} = \mathbf{F}_k \mathbf{y}_k - \mathbf{U}_{k+1,k} + \mathbf{\Gamma}_k \mathbf{w}_k \quad (7)$$

where k is the discrete-time index,

$$\mathbf{F}_k = \begin{bmatrix} 1 & T_k & 0 & 0 & 0 & 0 \\ 0 & 1 & 0 & 0 & 0 & 0 \\ 0 & 0 & 1 & T_k & 0 & 0 \\ 0 & 0 & 0 & 1 & 0 & 0 \\ 0 & 0 & 0 & 0 & 1 & 0 \\ 0 & 0 & 0 & 0 & 0 & 1 \end{bmatrix}, \quad (8)$$

$$\mathbf{\Gamma}_k = \begin{bmatrix} T_k^2/2 & 0 & 0 & 0 \\ T_k & 0 & 0 & 0 \\ 0 & T_k^2/2 & 0 & 0 \\ 0 & T_k & 0 & 0 \\ 0 & 0 & T_k & 0 \\ 0 & 0 & 0 & T_k \end{bmatrix}, \quad (9)$$

$$\mathbf{U}_{k+1,k} = \begin{bmatrix} x^o_{k+1} - x^o_k - T_k \dot{x}^o_k \\ \dot{x}^o_{k+1} - \dot{x}^o_k \\ y^o_{k+1} - y^o_k - T_k \dot{y}^o_k \\ \dot{y}^o_{k+1} - \dot{y}^o_k \\ 0 \\ 0 \end{bmatrix}, \quad (10)$$

$\mathbf{w}_k$ is zero-mean Gaussian noise vector with covariance $\mathbf{Q} = \mathrm{diag}[q_x, q_y, q_\ell, q_\gamma]$ and T_k is the sampling interval. The matrix $\mathbf{U}_{k+1,k}$ is a vector of deterministic inputs which account for the observer acceleration.

2.2 Measurement equation

We assume that the sensor is a high-resolution radar, and that it supplies the tracking system with positional measurements (target range and bearing) in relation to the target centroid, as well as the target extent along the LOS. Then the measurement equation is nonlinear, i.e.

$$\mathbf{z}_k = \mathbf{h}(\mathbf{y}_k) + \mathbf{v}_k \quad (11)$$

where $\mathbf{z}_k$ is the measurement vector at time k, $\mathbf{h}(\mathbf{y}_k) = \begin{bmatrix} r(\mathbf{y}_k) & \theta(\mathbf{y}_k) & L(\phi(\mathbf{y}_k)) \end{bmatrix}^T$ with

$$r(\mathbf{y}_k) = \sqrt{(\mathbf{y}_k[1])^2 + (\mathbf{y}_k[3])^2} \quad (12)$$

$$\theta(\mathbf{y}_k) = \arctan\left(\frac{\mathbf{y}_k[3]}{\mathbf{y}_k[1]}\right) \quad (13)$$

$$L(\phi(\mathbf{y}_k)) = \mathbf{y}_k[5]\sqrt{\cos^2\phi + (\mathbf{y}_k[6])^2 \sin^2\phi} \quad (14)$$

The relationship between angle ϕ and the state vector $\mathbf{y}_k$ is given by:

$$\phi(\mathbf{y}_k) = \arctan\left(\frac{\mathbf{y}_k[1]\mathbf{y}_k[4] - \mathbf{y}_k[2]\mathbf{y}_k[3]}{\mathbf{y}_k[1]\mathbf{y}_k[2] + \mathbf{y}_k[3]\mathbf{y}_k[4]}\right). \quad (15)$$

Measurement noise $\mathbf{v}_k$ in (11) is assumed to be zero-mean Gaussian with covariance $\mathbf{R} = \mathrm{diag}[\sigma_r^2, \sigma_\theta^2, \sigma_L^2]$.

Two implicit assumptions are made in relation to the measurement equation. The first is that the target is moving (its velocity vector is non-zero). The second is that the target ellipse is oriented in such a manner that its major axis is parallel to the target velocity vector.

Note that the idea of using an ellipse to represent an extended object (or a cluster of closely spaced objects)

was originally proposed in [4]. The authors of [4], however, consider a filter which decouples ellipse parameters from target motion, whereas the key aspect of our approach is the coupling between the velocity vector and the orientation.

2.3 Initial state pdf

Nonlinear filtering is performed within the framework of sequential Bayesian estimation, which requires the initial pdf of the state vector to be specified. We assume that this initial pdf is Gaussian with covariance matrix

$$\mathbf{P}_0 = \text{diag}[\sigma_x^2, \sigma_{\dot{x}}^2, \sigma_y^2, \sigma_{\dot{y}}^2, \sigma_\ell^2, \sigma_\gamma^2]. \quad (16)$$

Here σ_x, $\sigma_{\dot{x}}$, σ_y, $\sigma_{\dot{y}}$ correspond to the way the nonlinear filter is initialised (one-point or two-point differencing [2]). The selection of σ_ℓ and σ_γ is based on prior knowledge of target classes expected to be active in the surveillance volume. Note that if the targets are ships, the prior on γ is very tight (i.e. σ_γ is small).

3 Cramer-Rao bound

The nonlinear filtering problem defined by equations (7) and (11) does not have a closed form optimal solution and in practice must be implemented as an approximation. However, the theoretically best achievable tracking error performance (second-order error), in the form of the Cramér-Rao lower bound (CRLB) is readily available. Such a bound is very important as a tool for tracking algorithm assessment, performance prediction, tracking system design, sensor allocation and scheduling (see [5] and references therein).

3.1 Recursive computation

Let $\hat{\mathbf{y}}_k$ be an unbiased state estimator based on measurements $\mathbf{Z}_k = \{\mathbf{z}_1, \ldots, \mathbf{z}_k\}$. The covariance of $\hat{\mathbf{y}}_k$ has a lower bound expressed as follows:

$$\mathbf{C}_k \triangleq \mathbb{E}\left[(\hat{\mathbf{y}}_k - \mathbf{y}_k)(\hat{\mathbf{y}}_k - \mathbf{y}_k)^T\right] \geq \mathbf{J}_k^{-1} \quad (17)$$

where $\mathbf{J}_k$ is referred to as the *filtering* information matrix (FIM) defined in [14] [13], [15]. The inverse $\mathbf{P}_k = \mathbf{J}_k^{-1}$ is the Cramér-Rao lower bound (CRLB). The inequality in (17) means that the difference $\mathbf{C}_k - \mathbf{J}_k^{-1}$ is a positive semi-definite matrix.

If process noise if present, i.e. $\mathbf{w}_k \neq 0$ in (7), then $\mathbf{y}_k$ is unknown and random, and we seek the Posterior CRLB (PCRLB). Tichavsky et al. [13] provided a Riccati-like recursion for the calculation of $\mathbf{J}_k$ in this case. When state equation is linear and measurement equation is nonlinear (as in our case) the FIM is computed as:

$$\begin{aligned}\mathbf{J}_{k+1} =& \mathbf{Q}^{-1} - \mathbf{Q}^{-1}\mathbf{F}\left(\mathbf{J}_k + \mathbf{F}^T\mathbf{Q}^{-1}\mathbf{F}\right)^{-1}\mathbf{F}^T\mathbf{Q}^{-1} \\ &+ \mathbb{E}\left\{\mathbf{H}_{k+1}^T\mathbf{R}_{k+1}^{-1}\mathbf{H}_{k+1}\right\}. \end{aligned} \quad (18)$$

where $\mathbf{H}_k$ is the Jacobian of nonlinear measurement function $\mathbf{h}_k(\cdot)$, evaluated at the true state $\mathbf{y}_k$, i.e. $\mathbf{H}_k = \left[\nabla_{\mathbf{y}_k}\mathbf{h}^T(\mathbf{y}_k)\right]^T$. Thus an element of matrix $\mathbf{H}_k$ is defined as

$$\mathbf{H}_k[i,j] = \frac{\partial \mathbf{h}_k[i]}{\partial \mathbf{y}_k[j]}. \quad (19)$$

Clearly $\mathbf{H}_k$ depends on $\mathbf{y}_k$ and the expectation $\mathbb{E}$ in (18) is taken over $\mathbf{y}_k$. In the absence of process noise, recursion (18) simplifies to [12]:

$$\mathbf{J}_{k+1} = \left[\mathbf{F}_k^{-1}\right]^T \mathbf{J}_k\mathbf{F}_k^{-1} + \mathbf{H}_{k+1}^T\mathbf{R}_{k+1}^{-1}\mathbf{H}_{k+1}. \quad (20)$$

If the initial state pdf is Gaussian with covariance $\mathbf{P}_0$, the recursion (18) or (20) is initialised with $\mathbf{J}_0 = \mathbf{P}_0^{-1}$.

3.2 Jacobian $\mathbf{H}_k$

The Jacobian $\mathbf{H}_k$ is a 3×6 matrix. The non-zero elements of the first two rows are:

$$\mathbf{H}_k[1,1] = \frac{\mathbf{y}_k[1]}{\sqrt{\mathbf{y}_k^2[1] + \mathbf{y}_k^2[3]}} \quad (21)$$

$$\mathbf{H}_k[1,3] = \frac{\mathbf{y}_k[3]}{\sqrt{\mathbf{y}_k^2[1] + \mathbf{y}_k^2[3]}} \quad (22)$$

$$\mathbf{H}_k[2,1] = -\frac{\mathbf{y}_k[3]}{\mathbf{y}_k^2[1] + \mathbf{y}_k^2[3]} \quad (23)$$

$$\mathbf{H}_k[2,3] = \frac{\mathbf{y}_k[1]}{\mathbf{y}_k^2[1] + \mathbf{y}_k^2[3]} \quad (24)$$

The derivation of the first four elements of the third row is done by differentiation using the chain rule:

$$\mathbf{H}_k[3,j] = \frac{\partial L(\phi(\mathbf{y}_k))}{\partial \mathbf{y}_k[j]} = \frac{\partial L}{\partial \phi} \cdot \frac{\partial \phi}{\partial \mathbf{y}_k[j]} \quad (25)$$

for $j = 1, \ldots, 4$. It can be shown by differentiation that:

$$\begin{aligned}\frac{\partial L}{\partial \phi} =& \frac{\mathbf{y}_k^2[5](1 - \mathbf{y}_k^2[6])}{L(\mathbf{y}_k)} \cdot \frac{(\mathbf{y}_k[1]\mathbf{y}_k[2] + \mathbf{y}_k[3]\mathbf{y}_k[4])}{(\mathbf{y}_k^2[1] + \mathbf{y}_k^2[3])} \\ &\times \frac{(\mathbf{y}_k[1]\mathbf{y}_k[4] - \mathbf{y}_k[2]\mathbf{y}_k[3])}{(\mathbf{y}_k^2[2] + \mathbf{y}_k^2[4])} \end{aligned} \quad (26)$$

and

$$\frac{\partial \phi}{\partial \mathbf{y}_k[1]} = \frac{\mathbf{y}_k[3]}{\mathbf{y}_k^2[1] + \mathbf{y}_k^2[3]} \quad (27)$$

$$\frac{\partial \phi}{\partial \mathbf{y}_k[2]} = -\frac{\mathbf{y}_k[4]}{\mathbf{y}_k^2[2] + \mathbf{y}_k^2[4]} \quad (28)$$

$$\frac{\partial \phi}{\partial \mathbf{y}_k[3]} = -\frac{\mathbf{y}_k[1]}{\mathbf{y}_k^2[1] + \mathbf{y}_k^2[3]} \quad (29)$$

$$\frac{\partial \phi}{\partial \mathbf{y}_k[4]} = \frac{\mathbf{y}_k[2]}{\mathbf{y}_k^2[2] + \mathbf{y}_k^2[4]} \quad (30)$$

The last two elements of the Jacobian are:

$$\mathbf{H}_k[3,5] = \sqrt{\cos^2\phi + \mathbf{y}_k^2[6]\sin^2\phi} \quad (31)$$

$$\mathbf{H}_k[3,6] = \frac{\mathbf{y}_k[5]\mathbf{y}_k[6]\sin^2\phi}{\sqrt{\cos^2\phi + \mathbf{y}_k^2[6]\sin^2\phi}} \quad (32)$$

4 Analysis of the CRLB

The CRLB for the described problem of extended target tracking depends on: (i) the covariance of the initial state pdf defined by (16); (ii) target-observer geometry; (iii) measurement accuracy; (iv) process noise. We restrict our analysis of CRLB to the zero process noise case, since we observed that small amounts of process noise have only negligible effect. The influence of the remaining three factors on the CRLB are examined using the following scenario.

The observer is located at the origin of $x-y$ plane. The target is at location $(3000, 3100)$ m, its length is $\ell = 50$ m and its aspect ratio is $\gamma = 0.2$. The observer is static, while the target is moving with constant speed of 10 m/s. The observer is measuring target range, azimuth and along-range target extent every $T_k = 0.2$ s. Each of these measurements is corrupted by zero-mean white Gaussian errors with (nominal) standard deviations: $\sigma_r = 5$ m, $\sigma_\theta = 0.2^o$ and $\sigma_L = 5$ m. The covariance matrix $\mathbf{P}_0$ of the initial state pdf has the following parameters:

$$\sigma_x = \sigma_y = 50 \text{ m} \quad (33)$$

$$\sigma_{\dot{x}} = \sigma_{\dot{y}} = 2 \text{ m/s} \quad (34)$$

$$\sigma_\ell = 20 \text{ m} \quad (35)$$

$$\sigma_\gamma = 0.03 \quad (36)$$

4.1 The influence of σ_L

Figure 2 shows the $\sqrt{CRLB}$ curves for $\dot{x}^t = -4.4$ m/s and $\dot{y}^t = 9$ m/s, corresponding to target: (a) position; (b) velocity; (c) length ℓ and (d) aspect ratio γ. Three different values of σ_L are considered: 0.1 m (thick solid line), 5 m (dashed solid line) and 100 m (thin solid line). The first value of σ_L corresponds to unrealistically accurate measurements, the second value is of practical interest and the third value mimics the case when the measurement L is not available.

Figure 2.(a) shows that the measurements of target extent along the LOS are of small importance for the estimation of target position. Note that the dashed horizontal line in this figure (approximately at 16 m) corresponds to the sensor positional accuracy. Similarly, Figure 2.(b) indicates that measurements of L make a very small impact on the estimation of target velocity. However, the impact of measurement L on the estimation accuracy of target length, shown in Figure 2.(c), is quite dramatic both for $\sigma_L = 0.1$ m and for $\sigma_L = 5$ m. Finally, the $\sqrt{CRLB}$ curves for aspect ratio, see Figure 2.(d), are constant (based on initial pdf) for $\sigma_L = 5$ and 100 m. Only for very accurate measurements of L (at $\sigma_L = 0.1$ m) this error curve drops significantly over time.

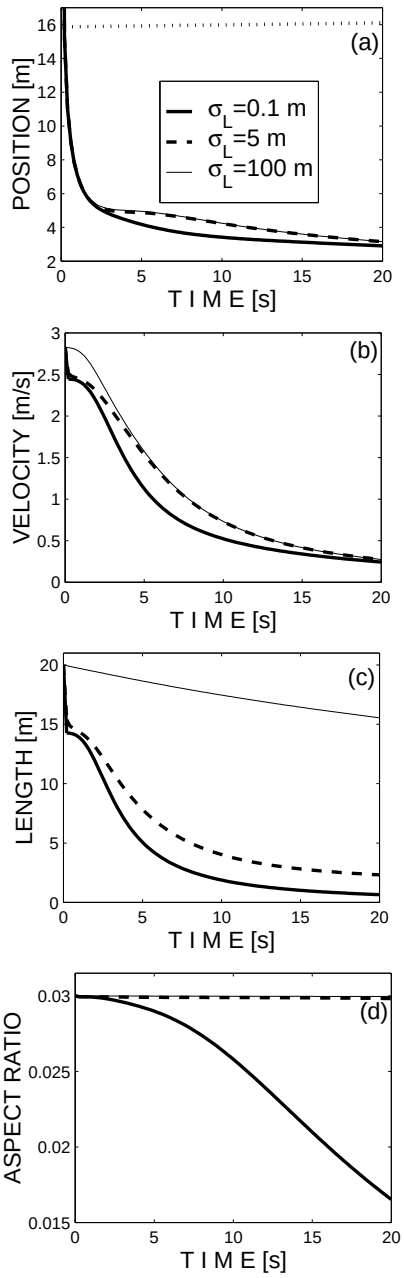

Fig. 2: $\sqrt{CRLB}$ curves for target (a) position; (b) velocity; (c) length ℓ and (d) aspect ratio, as a function of σ_L

4.2 The influence of ϕ

Next we analyse the impact of angle ϕ on CRLB. For this, we keep the experimental setup fixed and identical to the one considered before. The value of $\sigma_L = 5$ m is

fixed, but $\dot{x}^t$ and $\dot{y}^t$ are varied so that ϕ at $k=1$ takes values: 0^o, 45^o, 90^o, 135^o and 180^o (N.B. target speed $\sqrt{(\dot{x}^t)^2+(\dot{y}^t)^2}$ is always kept constant at 10 m/s). The effect of ϕ on $\sqrt{CRLB}$ curves for position and velocity is negligible and therefore we do not show these curves. The effect of ϕ on $\sqrt{CRLB}$ curves for estimation of L and γ is shown in Figure 3.(a) and (b) respectively. In

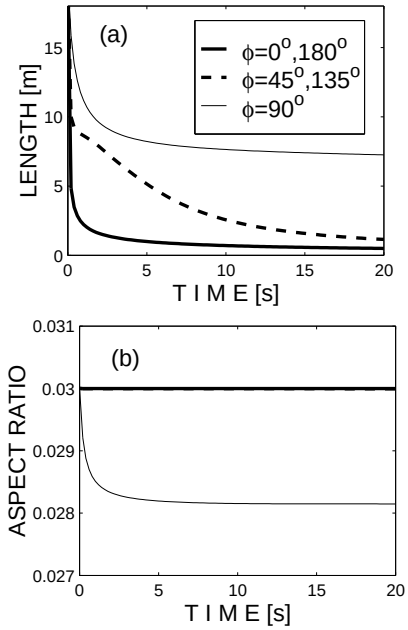

Fig. 3: $\sqrt{CRLB}$ curves for target (a) length ℓ and (b) aspect ratio γ, as a function of angle ϕ

relation to Figure 3 we observe that angle ϕ has quite a dramatic impact on the estimation accuracy of target length – the value of $\sqrt{CRLB}$ at $\phi = 90^o$ is almost 10 times higher than at $\phi = 0$. From this result it follows that for a moving observer (e.g. airborne platform) it makes sense to design an optimal ownship trajectory (optimal in the sense that it minimises the CRLB for length ℓ): the speed and heading of the observer should be such that angle ϕ approaches the value of 0 or 180^o (whichever is more convenient) as soon as practically possible.

4.3 The influence of σ_γ

Finally let us examine the impact of prior knowledge of the aspect ratio γ. Figure 4 shows the $\sqrt{CRLB}$ curves for target length and aspect ratio estimates when $\sigma_\gamma = 0.03$ and $\sigma_\gamma = 0.1$. Since the value of σ_γ did not make any effect on the CRLB for target position and velocity estimates, these curves are not shown. Figure 4 confirms the importance of a good prior for the estimation of target shape parameters. However, from the CRLB point of view, the target joint kinematic-shape state vector $\mathbf{y}_k$ is always observable (even when $\sigma_\gamma = 0.1$). What the CRLB does not show is that when the prior is vague, a practical recursive Bayesian nonlinear filter may become unstable and could diverge from the true state. This will be analysed in the next section.

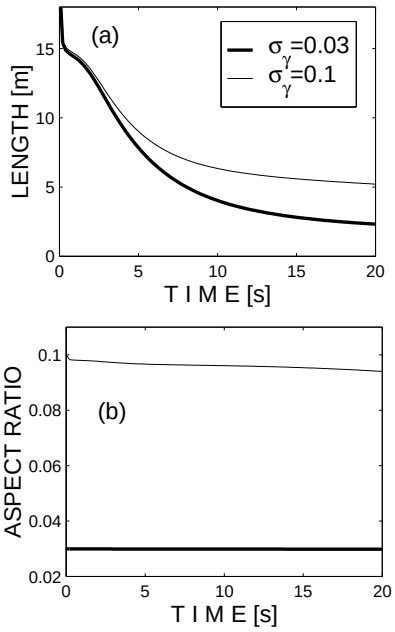

Fig. 4: $\sqrt{CRLB}$ curves for target (a) length ℓ and (b) aspect ratio γ, as a function of prior on γ

5 Nonlinear filters

Two recursive suboptimal Bayesian filters are designed for the described nonlinear filtering problem: the extended Kalman filter (EKF) and the unscented Kalman filter (UKF).

Since we adopted a linear state equation, the prediction in both EKF and UKF is performed as in the standard Kalman filter. The EKF uses the first order terms in the Taylor series expansion of the nonlinear measurement equation (11) to perform the filter update [2]. The resulting Jacobian of nonlinear measurement function, whose analytic expression was given in Sec.3.2, is evaluated at the prediction $\hat{\mathbf{y}}_{k|k-1}$.

The UKF is a recursive minimum mean square error estimator that uses the *true* nonlinear measurement model and approximates the probability density function of the state vector [9, 6]. This density, however, is assumed Gaussian (in reality it is not) and is represented by a set of deterministically chosen sample or *sigma* points. A particular choice of sigma points guarantees an accurate representation of the mean and covariance of any distribution for up to the second order of nonlinearity.

A small amount of process noise, as in (7), was applied in both EKF and UKF, in order to improve filter convergence. The covariance matrix of process noise is $\mathbf{Q} = \mathrm{diag}[q_x, q_y, q_\ell, q_\gamma]$, with $q_x = q_y = 2.5 \cdot 10^{-3}$ and $q_\ell = q_\gamma = 2.5 \cdot 10^{-11}$.

5.1 RMS Error Analysis

This subsection reports the RMS estimation error for the EKF and UKF. All error performance curves were obtained by averaging over 200 independent Monte Carlo runs. The target-observer geometry, the covariance $\mathbf{P}_0$, and the sensor parameters is the same as

described in Sec.4, with $\dot{x}^t = -4.4$ m/s and $\dot{y}^t = 9$ m/s; $\sigma_L = 5$ m; and $\sigma_\gamma = 0.03$.

Figure 5 shows the resulting RMS errors of EKF and UKF against the theoretical $\sqrt{CRLB}$ curves (the mean errors are close to zero in all cases). We observe that for target position and velocity, the RMS errors of both EKF and UKF are very close to their respective theoretical bounds. However, for target length and aspect ratio, the RMS errors of the EKF are significantly worse than their respective bounds. The UKF error performance is better than that of the EKF, but we note that its RMS error in aspect ratio is *growing* with time, indicating its inability to perform filtering in this dimension.

5.2 Consistency Tests

Both EKF and UKF provide in addition to state estimates $\hat{\mathbf{y}}_{k|k}$, a self assessment of their estimation errors in the form of the covariance matrix $\mathbf{P}_{k|k}$. A filter is referred to as being consistent if its covariance matrix is equal to the actual mean square error (MSE) matrix [2]. The most common statistical test for filter consistency is based on the average normalised estimation error square (NEES), defined as:

$$\bar{\epsilon} = \frac{1}{M \cdot n_y} \sum_{j=1}^{M} [\mathbf{e}_k^j]^T \, [\mathbf{P}_{k|k}^j]^{-1} \, \mathbf{e}_k^j \qquad (37)$$

where $\mathbf{e}_k^j = \hat{\mathbf{y}}_{k|k}^j - \mathbf{y}_k$ is the estimation error in j-th Monte carlo run, $j = 1, 2, \ldots, M$; and $n_y = 6$ is the state vector dimension. The consistency test assumes that estimation errors are zero-mean Gaussian. The average NEES of (37) should be $\chi^2_{n_y M}$ random variable with $n_y M$ degrees of freedom: its mean value is 1 and variance is $2/(n_y M)$. The filter is accepted as being consistent at level α if $\bar{\epsilon} \in [r_1, r_2]$ with probability $1 - \alpha$. The limits of the acceptance interval, r_1 and r_2 are calculated at level $\alpha = 0.05$ (i.e. acceptance with probability 0.95) as follows [2]:

$$r_{1,2} \approx \frac{1}{2n_y M} \left(\pm 1.96 + \sqrt{2n_y M - 1} \right)^2 . \qquad (38)$$

The result of the described consistency test for $\alpha = 0.05$ and $M = 200$ Monte Carlo runs (the same runs that were used to compute RMS errors in Sec.5.1) is shown in Figure 6. The acceptance limits of the consistency test are $r_1 = 1.0812$ and $r_2 = 0.9212$. We observe that both filters are inconsistent; moreover, since the average NEES exceeds the upper limit ($\bar{\epsilon}_k > r_1$), we know that both filters are *overoptimistic*. This means that filter calculated covariances are too small compared to the actual MSE. This type of behavior often leads to filter divergence, which was indeed occasionally observed for both EKF and UKF. Note that the average NEES curve of UKF is closer to the acceptance interval $[r_1, r_2]$ than the NEES curve of the EKF; in practice this means that the UKF is less prone to divergence than the EKF.

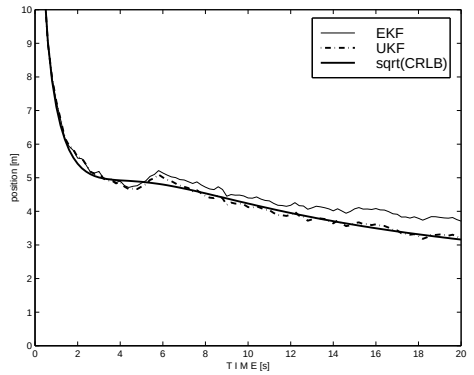

(a)

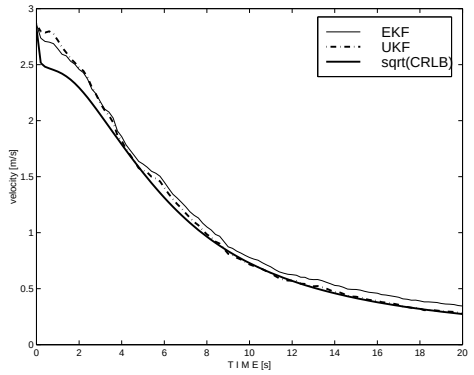

(b)

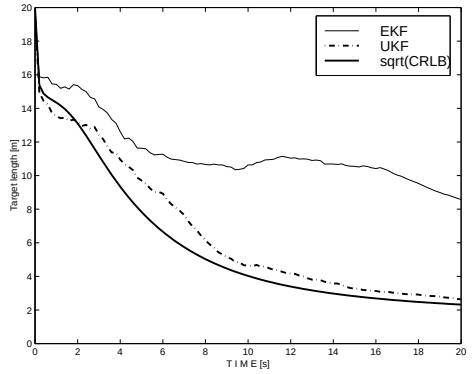

(c)

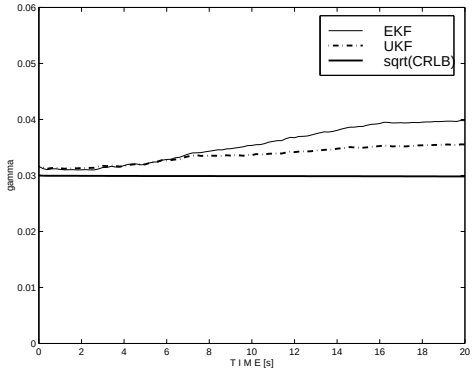

(d)

Fig. 5: RMS error curves of EKF and UKF against the $\sqrt{CRLB}$ curves for: (a) target position, (b) velocity, (c) length ℓ and (d) aspect ratio γ

.

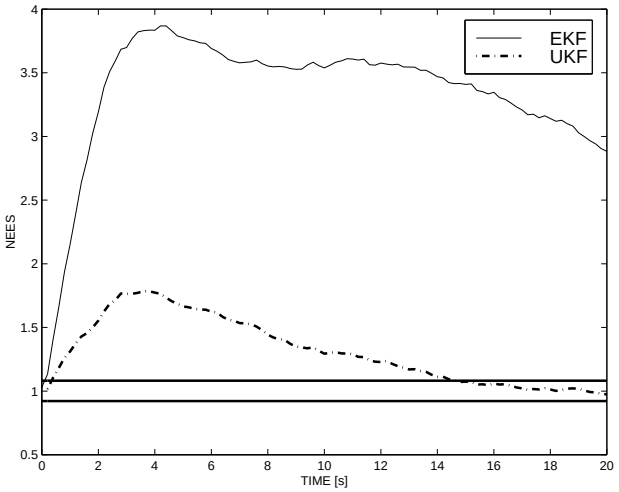

Fig. 6: Average NEES for EKF and UKF; the solid horizontal lines indicate the consistency test acceptance limits.

Remark 1. The CRLB analysis shows that measurements of target extent along the LOS are having a very small impact on the estimation accuracy of target position and velocity, for realistic value of $\sigma_L = 5$ m. Hence, it would be possible to decouple position/velocity estimation from length/aspect-ratio estimation. The most convenient implementation of position/velocity estimation would be based on consistent unbiased conversion of range-bearing into the Cartesian measurements [7], followed by the Kalman filter. The estimation of length/aspect-ratio would then follow using either a nonlinear filter or some parameter estimation technique (e.g. maximum likelihood estimation).

Remark 2. Additional measurements of target angular extent, if available, would improve the estimation accuracy of target length and aspect ratio.

6 Conclusions

The paper studied a nonlinear filtering problem for tracking an extended target whose shape is modelled by an ellipse, using the measurements of target extent along the line of sight, in addition to the usual positional measurements. The Cramér-Rao lower bounds are examined and the influence of measurement accuracy, target-observer geometry and the uncertainty in aspect ratio are investigated. Two simple nonlinear filters (extended and unscented Kalman filters) have been developed for this problem and their performance studied based on Monte Carlo simulations. It appears that both EKF and UKF are not suitable for this nonlinear filtering problem, because the nonlinearity involved is too severe. The UKF, however, shows much better performance than the EKF. It is left for future work to develop a particle filter for this application and to examine its performance. The particle filter could be applied only to the two-dimensional problem of target length and aspect-ratio estimation.

Acknowledgements

B. Ristic would like to thank IRIDIA, Université libre de Bruxelles, for being his host while the research presented in this paper has been carried out.

References

[1] Y. Bar-Shalom and X. R. Li. *Multitarget-Multisensor Tracking*. YBS, 1995.

[2] Y. Bar-Shalom, X. R. Li, and T. Kirubarajan. *Estimation with Applications to Tracking and Navigation*. John Wiley & Sons, 2001.

[3] J. Dezert. Tracking manoeuvring and bending extended target in cluttered environment. In *Proc. of SPIE*, volume 3373, pages 283–294, 1998.

[4] O. E. Drummond, S. S. Blackman, and G. C. Petrisor. Tracking clusters and extended objects with multiple sensors. In *Proc. SPIE*, volume 1305, pages 362–375, 1990.

[5] M. Hernandez, B. Ristic, A. Farina, and L. Timmoneri. Comparison of two Cramér-Rao bounds for non-linear filtering with $P_d < 1$. *IEEE Trans. Signal Processing*, to appear in 2004.

[6] S. Julier, J. Uhlmann, and H.F.Durrant-White. A new method for nonlinear transformation of means and covariances in filters and estimators. *IEEE Trans. Automatic Control*, 45(3):477–482, March 2000.

[7] D. Lerro and Y. Bar-Shalom. Tracking with debiased consistent converted measurements versus EKF. *IEEE Trans. Aerospace and Electronic Systems*, 29(3):1015–1022, July 1993.

[8] M. R. Morelande and S. Challa. An algorithm for tracking group targets. In *Proc. Workshop on Multiple Hypoteses Tracking: A Tribute to S. Blackman*, San Diego, USA, May 2003.

[9] B. Ristic, S. Arulampalam, and N. Gordon. *Beyond the Kalman filter: Particle filters for tracking applications*. Artech House, 2004.

[10] D. J. Salmond and N. J. Gordon. Group and extended object tracking. In *Proc. SPIE*, volume 3809, 1999.

[11] D. J. Salmond and M. C. Parr. Track maintenance using measurements of target extent. *IEE Proc. Radar Sonar Navigation*, 150(6), December 2003.

[12] J. H. Taylor. The Cramer-Rao estimation error lower bound computation for deterministic nonlinear systems. *IEEE Trans. Automatic Control*, 24(2):343–344, April 1979.

[13] P. Tichavsky, C. H. Muravchik, and A. Nehorai. Posterior Cramér-Rao bounds for discrete-time nonlinear filtering. *IEEE Trans. Signal Processing*, 46(5):1386–1396, May 1998.

[14] H. L. VanTrees. *Detection, Estimation and Modulation Theory (Part I)*. John Wiley & Sons, 1968.

[15] M. Šimandl, J. Královec, and P. Tichavský. Filtering, predictive and smoothing Cramér-Rao bounds for discrete-time nonlinear dynamic systems. *Automatica*, 37:1703–1716, 2001.